

## 9. BASIN-FILLING MODELS

### A. INTRODUCTION

Up until now, this course has mainly focused on subsidence in sedimentary basins—how it occurs, and how it can be determined as a function of time over the history of a basin. The pattern of subsidence in time and space largely determines the gross geometry of time-bounded sedimentary units because it controls the rate at which space is created for sedimentation (accommodation potential). On a finer scale, however, the pattern of subsidence plays a major role in determining the distribution of facies types within the sedimentary fill of the basin. The relation between patterns of subsidence and the internal character of the sediments can be understood through the use of basin-filling models, which we will study in this section. Basin-filling modeling, along with a variety of other quantitative techniques, has recently been referred to as "quantitative dynamic stratigraphy", which can be read about in a new book by the same name (Cross, 1990). The development and application of basin-filling models is a subdiscipline that is still in its infancy, so the emphasis in this section of the course will be on the principles underlying various approaches, how the models are constructed, and the kinds of things they tell us, rather than on specific case studies and standard techniques. Because the necessary mechanics are understood better for streams than for any other sedimentary system, much of our effort will focus on sedimentation in alluvial systems.

Given our present state of ignorance of many of the basic processes of basin filling, it is reasonable to ask whether or not it is worth even attempting to apply the knowledge we have to constructing formal theoretical models for sedimentary basins. Don't these models have so many assumptions, restrictions, and simplifications that they can never possibly describe the real world? In many senses, the answer is yes—modeling and theory certainly do not play the same role in stratigraphy that they do in chemistry and physics. We are dealing with systems with an enormous number of degrees of freedom, and so we have to think about the uses of models in a somewhat different light than in the more fundamental sciences. Here are some of the ways in which we see models being used now and in the near future:

(1) They are a means of generalizing. One can always develop an empirical model based on observations from a specific basin and be guaranteed that the model is "correct"; the problem is that it is unlikely to apply anywhere else. The appeal of quantitative models such as those we discuss in this chapter is that they are based on basic laws governing sediment dynamics, so they are very general. The tradeoff is that they involve so many assumptions and simplifications that they can hardly be expected to apply exactly anywhere! One way of resolving this apparent conflict is to think of a given real basin as a kind of convolution of general processes with specific local conditions. The models being developed are an attempt to clarify the general processes, with the understanding that local effects can be resolved only through detailed field work. An example of this is the use of stratigraphic models in the oil industry for intelligent extrapolation or interpolation of existing data. In effect, the data provide the necessary local framework for application of the models.

(2) They are a means of exploring the effects of varying parameters in complex systems. As you will see presently, the behavior of even very simple stratigraphic models can be complex and nonintuitive. Although we all look forward to the day when quantitative stratigraphic models offer strong, rigorously testable predictions, the best use of the primitive models available now may well be to help us in our conceptual thinking. Even the process of setting up a model is educational. What are the basic governing variables in a sedimentary system? What happens when one or more of them vary along any given trajectory? We can sharpen our intuition by exploring the answers to questions like these.

(3) They are a means of organizing field projects. As you will see, stratigraphic models may suggest interesting critical relations that can be sought after in the field. They also give us with some idea of what kinds of spatial and temporal resolution are needed to observe predicted effects.

## B. STRATEGY

### 1. *Dependent and Independent Variables*

The first requirement in setting up any model is to determine the dependent (calculated) and independent (specified) variables. For basin-filling models, the range of possible dependent variables is large, but some obvious possibilities include grain-size variation across the basin and the locations of major facies breaks such as the alluvial-marine transition or the transition from high-energy to low-energy facies. For alluvial systems, the latter might be refined to include, for instance, predictions of channel depth and characteristic primary internal structures.

For most types of basin, the basic independent variables include the pattern of subsidence over the basin, the locations of all sediment sources, and the rate and grain-size distribution of sediment supplied for each source. For alluvial systems, additional important variables are the distribution of rainfall over the basin and its source areas and eustatic sea level. All of the above are functions of time. Other variables, such as climatic influences on vegetation, may be important but are so poorly understood that it is inappropriate to include them in the crude first-order models that are now under development. For marine systems, major additional independent variables include the wave climate, distribution of wind-driven currents, eustatic sea level, and the various biogeochemical factors that influence carbonate sedimentation.

The next step is to devise a model that relates the dependent variables to the independent variables. Running such a model through time then produces a synthetic stratigraphy that can be compared with that of real basins. At their present fairly primitive level of development, basin-filling models are mainly useful as qualitative guides for our intuition rather than as quantitative predictive tools. They give us some idea of how a complex system with several interacting components will behave as the inputs (independent variables) vary.

## *2. Geometric and Dynamic Models*

Basin-filling models can be classified as either geometric or dynamic. The distinction really represents two different approaches to model building. Before discussing these two approaches, it is helpful to consider briefly some basic aspects of basin sedimentation.

In the absence of subsidence, all sediment-transport systems except for the deep oceans tend toward an equilibrium state in which they transport all the sediment supplied to them through without loss. This is called the graded state in rivers, but it can exist in any transport system. The fundamental effect of subsidence on the transport system is to induce deposition through a variety of mechanisms. This obviously makes attainment of grade as defined above impossible. But in general, the system will tend toward a different equilibrium in which the rate of deposition at each point is equal to the subsidence rate (Fig. 9.1). The surface topography adjusts itself until the rate of deposition and subsidence rate are in balance and then remains constant. In these notes, we will refer to systems in which subsidence and sedimentation are in balance as being in equilibrium. Grade is then a special kind of equilibrium for which the subsidence rate is zero. Determination of the characteristics of equilibrium transport systems as functions of the independent variables listed above is of fundamental importance in understanding basin filling.

The constant surface geometry characteristic of equilibrium systems is the starting point of what have been termed geometric models. In general, a geometric model is any one that begins by specifying the geometry of the depositional system (as opposed to calculating it as part of the model). The model is used to determine the geometry of the sediment fill in terms of the specified system geometry. A good example of a geometric model is that of Pitman for coastal-plain deposition under fluctuating sea level, discussed in Chapter 8. There, it was assumed that the transport system maintains a fixed slope against subsidence. Although this kind of assumption is, in principle, untenable for many systems, geometric models have the advantage of being simple to construct, and, as you have seen, they can give predictions that are at

least qualitatively reasonable for the overall geometry of major sedimentary units.

The alternative to geometric models is to use some form of approximation to the basic laws that govern sediment transport and deposition. These are termed dynamic models. Construction of a dynamic model must begin with consideration of the transport of sediment in the basin. The spatial distribution of sediment transport rate  $q_s$  can be described by a vector field in which the length of each arrow gives the volume rate of sediment transported past that point per unit time. The rate of transport is determined by properties of the flow and of the sediment available in the bed. The fundamental connection between deposition and sediment transport is provided by the continuity (conservation of mass) equation for sediment :

$$\sigma + \frac{\partial \eta}{\partial t} = \frac{-1}{C_0} \left[ \frac{\partial q_{sx}}{\partial x} + \frac{\partial q_{sy}}{\partial y} \right] \quad (9.1)$$

where  $\eta$  is the elevation of the sediment surface above a fixed datum,  $\sigma$  the subsidence rate,  $t$  time,  $C_0$  the volume concentration of sediment in the bed,  $q_s$  the sediment flux in volume per unit width per unit time, and  $x$  and  $y$  longitudinal and lateral horizontal coordinates, respectively (Fig. 9.2).

The right-hand side expresses the fact that, on average, sediment is deposited at some location only if more material is brought in from upstream than is removed downstream. Equation 9.1 implies that in a depositional system the transport rate must generally decrease going down the direction of transport. In a subsiding system at equilibrium,  $\partial h / \partial t = 0$ , and thus the subsidence pattern is directly linked to the sediment-transport field. If the relation between the transport rate and other properties of the system (e.g., channel depth and width, flow velocity) is understood, equation 9.1 provides the first step in predicting how these properties vary down the system as well. Thus, in modeling basin filling, we use information about the rate of deposition to determine how the flow field varies. It is interesting to note that this is exactly the opposite of what is normally done in engineering and quantitative

geomorphology: there one knows the flow field and uses it to find the distribution of rate of deposition.

One might ask whether or not dynamic models are better than geometric models. Naturally, a geometric model, which assumes away all the dynamics of the system, can never give predictions at the level of detail that a dynamic model can. (Imagine trying to predict the weather by assuming a fixed geometry for frontal systems.) On the other hand, accurate, general dynamic models are still a long way away (think about the accuracy of weather forecasting, which in many ways is a much simpler problem than filling a basin), and for many purposes geometric models are sufficient.

You have already seen a geometric model for stratigraphy generated by sea-level change on continental margins (Chapter 8). In this section of the course, we will look at examples of both geometric and dynamic models of fluvial deposition.

## C. ALLUVIAL SYSTEMS

The first example of a basin-filling model that we will examine in this course is a simple geometric model for gravel transport in an alluvial basin. After that, we will develop a dynamic model for alluvial systems that is based on the fundamental governing equations for flow and sediment transport in rivers. In both models, we will assume that the basin is two dimensional with only one sediment source.

### 1. *Geometric Models*

The purpose of this model is to study the cross-sectional shape of gravel bodies in alluvial basins as a function of the distribution of subsidence. We divide the sediment supply to the basin into two fractions: gravel (fraction =  $f_g$ ) and sand (fraction =  $1-f_g$ ).

When sediment comprising a mixture of sizes is deposited, there is a tendency for the least transportable material (usually coarser) to be deposited preferentially. This is called selective deposition. Thus, as a river system deposits sediment in response to subsidence, it tends to

deposit the coarser fraction first, leaving finer material to be carried on by the flow. This process can be thought of as a kind of depositional size fractionation. Its importance is implied by the observation that systems with high rates of deposition tend to have much higher rates of downstream fining than systems with low rates of deposition (e.g., Shaw and Kellerhals, 1982). These rates are often orders of magnitude higher than those associated with fining by abrasion, and so for present purposes abrasion will be ignored (although for discussion of how abrasion and selective deposition can be combined see Paola (1988)).

The mechanism of this sedimentary fractionation is still not well understood, but we can understand its general effect by assuming that a river system carrying gravel and sand sorts the gravel out perfectly. That is, it deposits only gravel until all the gravel in the supply is exhausted. In this case mass conservation for the gravel can be expressed as:

$$f_g(0) = \frac{R \int_0^{L_g} \sigma(x) dx}{\int_0^L \sigma(x) dx} \quad (9.2)$$

where  $R$ , the capture ratio, is the ratio of total rate of creation of area in the basin to rate of sediment supply, both in units of length<sup>2</sup>/time;  $L_g$  is the distance to which gravel is transported in the basin;  $L$  the total length of the basin;  $\sigma$  the subsidence rate; and  $x$  downstream distance with  $x = 0$  at the upstream end of the basin.

This relation is illustrated in Figure 9.3. Even for this very simple model, the gravel transport distance  $L_g$  is controlled by several factors. Equation 9.2 shows that areally extensive gravels (i.e., large  $L_g$ ) are to be expected where either subsidence rates near the source area are low or the rate of gravel supply is high. Alternatively, if the subsidence rate near the source area is high, most of the gravel is removed near the source, and the gravel deposit tends to be thick but not very areally extensive.

Figure 9.4 is a general illustration of this, and it shows that extensive, sheet-like gravel bodies are generally located in basins in which accumulation rates are low. You can also see that under these circumstances the gravel tends to be dominated by relatively durable clast types like quartzite and chert. This is because large transport distances and long transport times effectively remove easily abraded clasts by abrasion and weathering.

The tendency of rapidly subsiding basins to fractionate gravel out rapidly leads to the ambiguity in the relation between tectonic activity and the presence of gravel in the stratigraphic section that was discussed in Chapter 7. If the primary effect of increased tectonic activity in the sediment source area is to increase the rate of supply of gravel to the basin, then the tectonic activity is recorded as a coarsening-upward event. Conversely, if the dominant effect is to increase the subsidence rate (as is expected, for instance, where thrusting occurs on relatively weak lithosphere) then the sedimentary record of tectonism is upward fining (Heller et al., 1988).

Another illustration of the effect of subsidence distribution on downstream fining is shown in Figures 9.5 and 9.6. Figure 9.5 shows the distribution of thickness and grain size for Silurian gravels of eastern Pennsylvania. As expected in a foreland basin, the deposit thickens rapidly near the source area. You can see that this rapid thickening is accompanied by rapid grain-size decrease. On the other hand, Figure 9.6 shows similar data from a Triassic rift basin in southern Germany (middle Bunter sandstone), for which the sedimentation rate increases going into the basin. The grain-size data show that the size decreases slowly near the source, but then the rate of fining increases as the sedimentation rate increases.

## *2. Dynamic Models*

Relatively simple dynamic models for filling alluvial basins have been reported recently by Flemings and Jordan (1989), Jordan and Flemings (1990), and Paola (1990). These models use a somewhat similar strategy that will be discussed in the next section. A much more complex approach

to modeling has been presented by Tetzlaff and Harbaugh (1989) and will be discussed later.

The simplest basis on which a dynamic model of alluvial deposition can be constructed is the linear diffusion equation. The diffusion metaphor has long been applied in geomorphology and civil engineering to model the long-term behavior of river systems (Adachi and Nakatoh, 1969; Begin, 1987; Garde et al., 1981; Gill, 1983; Jain, 1981; Jaramillo and Jain, 1984; Ribberink and van der Sande, 1985; Soni, 1981; Zhang and Kahawita, 1987). We will begin our investigation of this approach to basin filling with a careful derivation of the diffusion equation itself, so you can see what assumptions are required. They are quite substantial! Knowing what the assumptions are is essential to applying such models wisely.

Consider a two-dimensional slice of a sedimentary basin, such as that shown in Figure 9.7. By two-dimensional, we mean that the rates of subsidence and of sediment supply do not vary across the direction of transport. We also assume that the water discharge does not vary downstream; although, this assumption is made mainly for convenience and can easily be relaxed.

Conservation of water mass in a single channel can be expressed as:

$$Q = bhu \quad (9.3)$$

where  $Q$  is water discharge,  $b$  is channel width,  $h$  is channel depth, and  $u$  is mean velocity. It is more useful to normalize discharge to unit basin width, giving:

$$q = \beta hu \quad (9.4)$$

where  $q$  is the total water discharge and  $\beta$  the total width of channels, both per unit width of basin.

For spatial scales that are long compared with those of the major topography in the river system (e.g., bars, channel bends), conservation of momentum can be written as:

$$\tau = -gh \frac{\partial \eta}{\partial x} \quad (9.5)$$

where  $\tau$  is the kinematic shear stress (force per unit area per unit fluid density),  $g$  is gravitational acceleration,  $\eta$  is elevation of the sediment surface relative to a fixed (nonsubsiding) horizontal datum, and  $x$  is downstream distance. This equation may be familiar to some of you. It says that the friction force exerted on the bed is just balanced by the downstream component of the weight of the fluid.

Conservation of mass for the sediment can be expressed as:

$$\sigma + \frac{\partial \eta}{\partial t} = \left( \frac{1}{C_0} \right) \frac{\partial (\beta \langle q_s \rangle)}{\partial x} \quad (9.6)$$

where  $\sigma$  is the subsidence rate (downward is positive),  $t$  is time,  $C_0$  is the volume concentration of sediment in the bed, and  $q_s$  is the rate of sediment transport per unit width of channel. For variables such as  $q_s$ , whose magnitude is strongly dependent on the time interval over which they are averaged (Sadler, 1981), we must be careful to specify long-term averages; this is denoted by angle brackets ( $\langle \rangle$ ). The problem of how to properly time-average equations such as 9.6 is a complex and subtle one that has received little attention in the geologic literature so far. The version shown above is a first approximation.

There is no explicit relation available for momentum conservation for sediment being transported by a moving fluid. The closest one can come is one of the many semiempirical relations that have been proposed (see the review in Brownlie (1981)). A simple relation due to Meyer-Peter and Müller (1948) can be written as:

$$q_s = \frac{8(\tau - \tau_c)^{3/2}}{g(s-1)} \quad (9.7)$$

where  $\tau_c$  is the critical shear stress needed to set the sediment in motion, which may be taken as a function of only the local mean sediment grain size, and  $s$  is the sediment specific gravity. Note that the quantities in

this equation are short-term averages; relations such as this one are known to apply only for short time scales. The simplest way around the problem of combining these with the long-term balance (equation 9.6) is to assume that the flow can be crudely characterized by a set of representative channel-forming conditions that occur intermittently. This intermittency is embodied in a time fraction  $I$ , so that, for example:

$$\langle q_s \rangle = Iq_s$$

This is clearly a gross simplification, but the price of added realism (e.g., treating the flow probabilistically and averaging over many realizations to get the long-term behavior) will be greatly increased computational complexity, added parameters that are difficult to constrain, and the blurring of interesting first-order effects.

Upon long-term averaging, equations 9.6 and 9.7 combine to yield:

$$\sigma + \frac{\partial \eta}{\partial t} = \left( \frac{-8I}{C_0 g(s-1)} \right) \frac{\partial (\beta (\tau - \tau_c)^{3/2})}{\partial x} \quad (9.8)$$

The shear stress can be related to the velocity by:

$$\tau = c_f u^2$$

where  $c_f$  is a drag coefficient, typically of order 0.01. In first-order models such as this one, it is usually taken to be constant.

At this point, two additional equations are required to solve the system. A natural choice for these is an independent relation between channel width and the other variables and an equation for mean grain size as a function of  $x$ , possibly in terms of the other variables in the system, which would determine  $\tau_c$ . However, there is no general relation available for stream width. Fortunately, the need to close the equations can also be met by postulating a relation between the actual shear stress  $\tau$  and the critical shear stress  $\tau_c$ . For gravel-bed rivers with noncohesive banks, a situation that is commonly associated with braiding, Parker (1978) demonstrated an interesting self-regulation mechanism for the stress at the channel center. The banks of such streams are extremely susceptible

to erosion. If the stress in the channel center rises above critical by more than a fixed, small amount, the banks begin to erode, widening the channel and, thus, reducing the stress in the center. The stress is maintained as:

$$\tau = (1 + \varepsilon)\tau_c \quad (9.9)$$

where  $\varepsilon$  is a constant. The theoretical value of  $\varepsilon$  is about 0.2; measured values are typically about 0.4 (Parker, 1978). We will refer to equation 9.9 loosely as the braided case.

On the other hand, streams with strong cohesive and/or vegetated banks can sustain shear-stress values that are much higher than critical, especially if they have sand beds. In this case, it is reasonable to assume  $\tau \gg \tau_c$  so that:

$$\tau - \tau_c \cong \tau \quad (9.10)$$

These conditions are likely to be met in deep, single-thread channels with well-developed flood plains, so we will refer to equation 9.10 loosely as the meandering case.

Introducing equation 9.9 or 9.10 into equation 9.8 gives:

$$\sigma + \frac{\partial \eta}{\partial t} = \left( \frac{-8IA}{C_0 g(s-1)} \right) \frac{\partial(\beta\tau^{3/2})}{\partial x} \quad (9.11)$$

where  $A = 1$  for the meandering case, and  $A = (\varepsilon/(1+\varepsilon))^{3/2}$  for the braided case. Using equations 9.5 and 9.8 and the definition of  $c_f$  given above, this reduces to:

$$\sigma + \frac{\partial \eta}{\partial t} = \nu \frac{\partial^2 \eta}{\partial x^2} \quad (9.12a)$$

which is the standard linear diffusion equation with  $\sigma$  appearing as a sink term and the diffusivity ( $\nu$ ) given by:

$$v = \frac{-8 \langle q \rangle A \sqrt{c_f}}{C_0 (s-1)} \quad (9.12b)$$

Note that for a given set of conditions,  $v$  has two values depending on the value of  $A$ . For a reasonable  $\varepsilon$  of 0.4, the braided-stream value of  $v$  is lower than the meandering-stream value by a factor of about 0.15. This reflects the common geomorphic wisdom that braided streams are generally less efficient than meandering streams: braided streams require a greater slope to transport the same load.

The drag coefficient ( $c_f$ ), the bed sediment concentration ( $C_0$ ), and the sediment specific gravity ( $s$ ) can be constrained by data from modern river systems and/or preserved sediments. In any case these parameters are not expected to vary much. Thus, the primary unknown, and the quantity that determines the order of magnitude of  $v$ , is the long-term average rate of water supply ( $\langle q \rangle$ ). This makes intuitive sense; it says that in wet basins, sediment is transported much more readily than in dry basins.

Within the framework of either the braided-stream or meandering-stream assumptions, equation 9.12 does not depend on grain size. As will be discussed below, the primary control on grain-size variation is the distribution of rate of deposition. The fact that equation 9.12 is independent of grain size means that it can be used to find the rate of deposition, from which the grain-size variation can be determined, with no need to iterate between the two.

Being of second order, equation 9.12 requires specification of two boundary conditions. The first involves the sediment flux at the upstream end of the system (Fig. 9.7). This can be set by coupling the depositional system to a diffusively eroding thrust front, as was done by Jordan and Flemings (1990), but here we will retain the sediment flux as an independent variable to give us greater flexibility (e.g., to allow for sediment sources not directly connected to the basin). Thus, at the upstream end ( $x = 0$ ) we have:

$$\langle q_s \rangle = v \frac{\partial \eta}{\partial x} \quad \text{at } x = 0 \quad (9.13a)$$

The form of the second boundary condition, applied at the downstream end ( $x = L$ ), depends on what assumption is made about the erodibility of the basement. Here, we assume that it is much less erodible than the basin fill. In this case, the boundary condition has two independent parts: the sediment flux must be zero, and the sediment thickness must also be zero (Fig. 9.7). Thus:

$$\frac{\partial \eta}{\partial x} = 0 \quad \text{and} \quad \eta = G \quad \text{at } x = L \quad (9.13b)$$

where  $G$  is the elevation of the basement. The presence of three boundary conditions in a second-order system allows determination of one additional variable, in this case, the length of the deposit  $L$  as a function of time.

### 3. *Modeling Grain-Size Variation*

It was long thought that the primary mechanism of downstream fining in rivers is abrasion of coarse clasts (Krumbein, 1941; Kuenen, 1956; Plumley, 1948). This view is partially substantiated by observations of systematic downstream change in clast composition in natural rivers, in which less durable clasts are progressively depleted (Abbott and Peterson, 1978; Shaw and Kellerhals, 1982). However, several workers (Brierley and Hickin, 1985; Shaw and Kellerhals, 1982) have pointed out that (1) observed rates of fining in natural rivers are often orders of magnitude higher than what appears possible for abrasion alone, based on tumbling-barrel experiments; and (2) the rate of fining increases with the rate of deposition, with the highest fining rates observed on rapidly aggrading alluvial fans. The first observation can be explained to some extent by invoking abrasion processes difficult to replicate in the laboratory (Bradley, 1970; Schumm and Stevens, 1973). However, the two observations together leave little room for doubt that selective deposition is the dominant cause of downstream fining in aggrading systems.

Unfortunately, very little is known of the actual mechanics of this selective-deposition process, although work is beginning on the problem (Paola and Wilcock, 1989). Only one hypothetical mechanism for selective deposition has been published at this time (Parker, 1989). Rather than attempting to incorporate an incompletely understood selective-deposition mechanism in our model, we will use the simple perfect-sorting approach employed in our geometric model above to embody the role of selective deposition in fractionating the input sediment. If we consider only two grain-size classes, for example gravel and sand, then we have the following close cousin of equation 9.2:

$$f_g \langle q_s \rangle = \int_0^{L_g} \left[ \sigma + \frac{\partial \eta}{\partial t} \right] dx \quad (9.14)$$

where  $f_g$  is the gravel fraction in the sediment supply.

#### 4. *Scaling the Equations*

It is not difficult to solve equations 9.12 and 9.13 using standard numerical methods (Press et al., 1986), but before doing so, it is helpful to apply a standard technique called nondimensionalization to equation 9.12 to give us a rough idea of what controls the relative sizes of each of its terms. We will adopt the characteristic scales  $h$ ,  $T$ ,  $\sigma_0$ , and  $L$  for  $\eta$ ,  $t$ ,  $\sigma$ , and  $x$ , respectively. This means that we expect  $\eta$ ,  $t$ ,  $\sigma$ , and  $x$  to have values that are of the order of these scale terms. Denoting nondimensional variables (which are all of order 1) with an asterisk, we have:

$$\sigma_0 \sigma_* + \left( \frac{h}{T} \right) \frac{\partial \eta_*}{\partial t_*} = \left( \frac{vh}{L^2} \right) \frac{\partial^2 \eta_*}{\partial x_*^2} \quad (9.15)$$

or, rearranging:

$$\frac{\sigma_0 L}{Q_s} \sigma_* + \left( \frac{L^2}{vT} \right) \frac{\partial \eta_*}{\partial t_*} = \frac{\partial^2 \eta_*}{\partial x_*^2} \quad (9.16)$$

where  $Q_s$  is a characteristic transport rate equal to  $vh/L$ . Note that two dimensionless numbers determine the magnitudes of the sink term and the time-dependent term relative to the spatial derivative on the right, which has been set to order 1. The first nondimensional number,  $\sigma_0 L/Q_s$ , is a measure of the rate at which cross-sectional area is created in the basin (numerator) relative to the rate of sediment transport and, thus, basin filling (denominator). The inverse of this number is similar to the capture ratio of Paola (1988), the ratio of sediment flux to the rate of creation of cross-sectional area in the basin. Roughly, if  $\sigma_0 L/Q_s > 1$ , the basin is underfilled; if  $< 1$ , the basin is overfilled and sediment exits the far end of the basin. In the limiting case of  $\sigma_0 = 0$ , no basin forms and equation 9.15 reduces to the standard diffusion equation as applied in geomorphic modeling.

The second dimensionless number on the left,  $L^2/vT$ , can be viewed as defining a natural time scale  $L^2/v$  for the basin. The presence of  $T$  in the denominator implies that if the basin is set up in some initial configuration and allowed to develop under constant conditions, it will evolve to an equilibrium configuration in which sedimentation balances subsidence, that is:

$$\sigma = v \frac{\partial^2 \eta}{\partial x^2} \quad (9.17)$$

This requires a time of the order of  $L^2/v$ . Thus, if the time scale  $T$  of any variations imposed on the basin (e.g., in sediment flux or water supply) is long relative to this natural response time, then the time-derivative term never becomes large compared with the other two terms. Equation 9.17 continues to apply (approximately), and the basin remains in quasiequilibrium as it responds to the imposed changes. We will refer to variations on time scales greater than and less than  $L^2/v$  as slow and rapid variations, respectively. We give an example calculation of the relevant scales in the next section.

By analogy with the results above, one might think that for rapid changes, for which  $T \ll L^2/\nu$ , the right-hand side of equation 9.16 (the spatial derivative) can be neglected. This cannot happen, however, because removing the spatial derivative will reduce the order of equation 9.16, and it will no longer satisfy all of its boundary conditions. The spatial term has been nondimensionalized to order 1. It can remain of comparable magnitude to the time-dependent term only if a new, smaller length scale ( $L'$ ) arises, such that  $(L')^2/\nu T$  is also of order 1.  $L'$  is the length scale over which the effects of the fluctuations are felt in the basin, so the extent of the basin that can be affected by fluctuating conditions at one of its boundaries is proportional to the square root of the period of the fluctuations. Note also that if  $L$  is replaced by the new reduced length scale  $L' = R(\nu T)$  in the scaling term  $\sigma L/Q_s$  for subsidence, this term becomes small relative to the other two as the time scale diminishes. Thus, as the time scale for imposed variations becomes short, equation 9.12 can be expected to behave increasingly like the classical diffusion equation without subsidence.

### 5. Estimation of Scales

As mentioned above, most of the elements of the diffusivity are fairly well constrained. Adopting as reasonable values  $c_r = 0.01$ ,  $C_0 = 0.7$ ,  $s = 2.7$ , and  $\varepsilon = 0.4$ , we have for the braided case  $\nu = 0.10\langle q \rangle$  and for the meandering case  $\nu = 0.67\langle q \rangle$ . The average water discharge per unit width of basin  $\langle q \rangle$  is  $rL_c$ , where  $r$  is the rainfall rate and  $L_c$  the length of the catchment area. (Note that we are ignoring downstream changes in  $\langle q \rangle$  due to rainfall along the basin itself.) For a catchment length of  $10^5$  m and a rainfall rate of 1 m/yr we have, for the braided case, a diffusivity of  $1 \times 10^4$  m<sup>2</sup>/yr and for the meandering case  $7 \times 10^4$  m<sup>2</sup>/yr. If the basin length is comparable to the catchment length ( $10^5$  m), the response time of the basin  $L^2/\nu$  is of the order of  $10^6$  yr in the braided case and  $10^5$  yr in the meandering case. In general, if the catchment length and the basin length are of a similar order of magnitude, the response times are of the order  $10L/r$  for the braided case and  $L/r$  in the meandering case.

## 6. Method of Solution

There are a variety of numerical methods available for solving equation 9.12a (Press et al., 1986); we use a fully implicit method to allow for long time steps. The major problem in solving the system (equation 9.12) is determining the length of the deposit for each time step. Usually, we can expect the boundary to be somewhere between the nodes of a predetermined grid, so a problem of this type cannot be solved exactly on a fixed spatial grid. In practice, positioning the boundary on the nearest node of a fixed grid produces acceptably small errors in mass conservation (typically a few percent over 100 time steps), provided the grid is reasonably fine. For the calculations discussed below, we used a grid with 100 spatial steps.

### D. MODEL RESULTS FOR QUASIEQUILIBRIUM CONDITIONS

We begin by presenting model results for slow (quasiequilibrium) variations, that is, those for which conditions vary on a time scale that is long compared with the natural response time of the basin,  $L^2/\nu$ . In the model runs, the diffusivity and basin length are those given above for the braided case ( $10^4$  m<sup>2</sup>/yr and  $10^5$  m, respectively). We consider variation in each of the four basic governing parameters: sediment flux, subsidence rate, gravel fraction in the sediment supply, and water supply (via the diffusivity  $\nu$ ). The variation is sinusoidal and occurs on a time scale of  $10^7$  years, which is 10 times the response time. The amplitude of the variation is 70% of the mean value in each case. In the model runs shown, the basin has a simple asymmetric distribution of subsidence, increasing linearly toward the sediment source. The mean value of the capture ratio is 1, so on average, the basin is just kept filled with sediment. We use equation 9.14 to determine the location of the transition from gravel to sand.

In all the runs in this and the next section, the basin is allowed to fill with sediment under constant conditions for a period equal to four times the response time before the variation is begun. This equilibration interval is always represented by the first two time lines in the fill. At the end of this period, the variation begins. Except for the sediment-flux case, each variable goes as  $\sin(2\pi t/T)$ , where  $t$  is time and  $T$  is the period

of the fluctuations. The sediment flux is varied as  $-\sin(2\pi t/T)$ . Once the variation begins, time lines are drawn every  $10^6$  yr.

### 1. *Variation in Sediment Flux*

Figure 9.8a shows the results of a model run as described above in which the sediment flux varies sinusoidally, and all other variables are held constant. Vertical sedimentation rates increase as flux increases, shown by an increase in spacing between isochrons on the diagram. Clastic progradation occurs (the position of the gravel-sand transition migrates toward the basin center) as the sediment flux increases. Clastic progradation over time is, of course, accompanied by an overall grain-size increase in any vertical section measured in the basin. Thus, this flux-driven style of progradation shows a positive correlation between sediment accumulation rate and grain size in vertical sections across the basin.

This scenario represents the traditional synorogenic interpretation of coarsening-upwards sections in alluvial basins (Rust and Koster, 1984). An increase in tectonic activity in the source area is a reasonable means of increasing the relief and, thus, the sediment flux to the basin, although an increase in flux can also result from changes in climate or source-rock lithology.

### 2. *Variation in Subsidence Rate*

A second model run (Fig. 9.8b) shows what happens if basin subsidence rate varies sinusoidally while the other variables remain constant. As subsidence begins to increase, more accommodation space is generated, trapping the supplied sediment in the most proximal part of the basin while the most distal sediments are eroded. The coarsest sediment, being the first to deposit, is localized in the extreme upstream end of the basin. Locally, vertical sedimentation rates in the proximal part of the basin increase as the gravel-sand transition migrates toward the head of the basin, as required by equation 9.14. The mean subsidence rate then decreases, space available for deposition decreases, and the gravel-sand transition progrades out across the basin. As in the previous case, this progradation is associated with change in grain size in any vertical

section. But for this subsidence-driven case, an increase in grain-size change upsection is associated with a reduction in vertical accumulation rate—exactly the opposite of the flux-driven case described above.

The subsidence-driven case, then, is one in which gravel progradation is linked to a reduction in local sediment accumulation rate. Assuming that subsidence is directly related to tectonic activity, in this case, gravel progradation represents periods of diminishing tectonic activity and is, therefore, not syntectonic in the traditional sense.

### 3. *Variation in Gravel Fraction*

A third end member worth noting is that in which gravel progradation is caused by an increase in the fraction of gravel in the sediment supply. Such a change can occur because of a change in source-rock lithology due to unroofing or faulting or a change in climate reducing the generation of fines by weathering. In this case (Fig. 9.8c), sediment flux and subsidence rate remain constant; thus, there are no changes in vertical accumulation rates coincident with a change in grain size upsection. In this distribution-driven model, there is no correlation between grain size and accumulation rate.

### 4. *Variation in Water Supply*

As discussed above, the amount of water available to the basin, controlled by the size of the catchment basin and the rainfall rate, is reflected directly in the diffusivity. The results of varying the diffusivity sinusoidally can be seen in Figure 9.8d. Although the amplitude of variation is just as large as for the variables discussed above, variation in diffusivity has no effect on the pattern of fill in the basin.

### 5. *Summary—Quasiequilibrium Variation*

Clearly, on quasiequilibrium time scales, changes in sediment flux, subsidence rate, and sorting cause the position of the gravel-sand front to shift smoothly back and forth across the basin. The end-member models discussed above are distinguished by the timing relation between grain size and vertical accumulation rate (Fig. 9.9). In the flux-driven case,

sedimentation rate and grain size change in phase with one another (Fig. 9.9a). For the subsidence-driven case, sedimentation rate and grain size are exactly out of phase (Fig. 9.9b). In the sorting-driven case, there is no phase relation between grain size and sedimentation rate (Fig. 9.9c). In contrast to these three cases, changes in water supply have no effect when applied over long time scales.

## E. MODEL RESULTS FOR NONEQUILIBRIUM CONDITIONS

What happens if the variations occur on time scales significantly less than the equilibrium time? The runs in this section were made under the same conditions as those above, except that the period of variation  $T$  is  $10^5$  yr, a factor of 100 less than those of the previous section and a factor of 10 less than the equilibrium time. The time lines are drawn every  $10^4$  yr.

### 1. *Variation in Sediment Flux*

The results of rapid variation in sediment flux are shown in Figure 9.10a; they are quite different from the quasiequilibrium case. During times of reduced sediment flux, there is erosion in the upstream part of the system as slopes are reduced to accommodate the decreasing flux. This results in the generation of proximal unconformities and the spreading of gravel far out into the basin. Thus, in contradistinction to the quasiequilibrium case (Fig. 9.8a), for rapid variations in sediment flux, gravel progrades during times of reduced sediment flux. Furthermore, the form of the gravel bodies is quite different. Even though the imposed variation is smooth and sinusoidal, the progradation takes place abruptly, leading to a distinctive sheet-like geometry. The retrogradation is even more abrupt, giving the whole cycle an asymmetric, coarsening-up form. In addition, the gravel is associated with pronounced proximal unconformities that weaken going out into the basin.

### 2. *Variation in Subsidence Rate*

In contrast to this, the results of rapid variation in subsidence rate are shown in Figure 9.10b. Even though the imposed variation in subsidence rate is just as strong as in the slow-variation case (Fig. 9.8b),

when it occurs rapidly relative to the equilibrium time, it produces almost no effect. The position of the gravel front barely moves, and there are no corresponding changes in the sedimentation rate.

### 3. *Variation in Gravel Fraction*

Rapid variation in supply gravel fraction, illustrated in Figure 9.10c, produces exactly the same effect as slow variation in gravel fraction; the gravel front progrades smoothly and continuously, and there are no accompanying changes in sedimentation rate.

### 4. *Variation in Water Supply*

The results of rapidly varying the diffusivity (and, thus, the rate of water supply) are shown in Figure 9.10d. In striking contrast to the analogous results for slow variation, rapid changes in diffusivity produce strong effects. These are similar to the effects of rapid variation in sediment flux. During times of increased diffusivity, as in times of reduced sediment flux, the proximal part of the deposit is planed off; the increased diffusivity allows the stream system to transport the imposed load on a reduced slope. This produces strong proximal unconformities and thin, extensive gravel tongues. As for variation in flux, the progradation is abrupt, even though the imposed variation is smooth and sinusoidal, and again has an asymmetric (coarsening-upward) vertical signature.

### 5. *Summary—Rapid Versus Slow Variation*

The most striking result of the model calculations is how much different the basin response is for rapid variation in imposed variables than for slow variation (except for the supplied gravel fraction, variation of which produces the same effect regardless of time scale). This distinction makes clear the fundamental role played by the response time in governing basin response to imposed variations, for it is the response time that determines what slow and rapid mean in real time. These results are summarized below:

Slow variation in sediment flux produces smooth progradation and retrogradation of the gravel front. Progradation occurs during times of

increased flux and is accompanied by increasing local sedimentation rate; we term this flux-driven coarsening. In contrast, rapid flux variation produces abrupt progradation of the gravel front during times of reduced flux to produce thin, extensive gravel sheets bounded below by strong proximal unconformities that die off into the basin. Although the gravel progrades abruptly, retrogradation is even faster, so that overall a coarsening-upward vertical signature results.

Slow variation in subsidence rate also produces smooth progradation and retrogradation of the gravel front. Progradation occurs during times of reduced subsidence and so is accompanied by reduction in local sedimentation rate; we term this subsidence-driven coarsening. In contrast, rapid variation in subsidence rate produces negligible effects on the sedimentation pattern. One might say that sedimentary basins are a kind of low-pass filter for variations in subsidence rate. The characteristic time for the filter is the response time as defined above. That is, it is controlled by the diffusivity and the basin length.

Slow and rapid variation in supplied gravel fraction produce similar effects; smooth progradation (during times of high gravel supply) and retrogradation with no accompanying changes in sedimentation rate.

Slow variation in water supply (diffusivity) produces no effect, but rapid variation produces abrupt progradational cycles, with extensive sheetlike gravel units being generated during times of high water supply. The overall pattern is one of coarsening-upward cycles capped by broad gravel tongues, similar to those produced by rapid variation in sediment flux. Sedimentary basins act as a kind of high-pass filter for variations in water supply. Again, the characteristic time for the filter is set by the response time as defined above.

## F. DISCUSSION

What causes the pronounced differences in the ways that the various governing parameters respond to changes in the time scale of variation? The answer to this can be found in the discussion of scaling effects presented above. There, we show that the long-term balance ( $T \rightarrow \infty$ ) is basically between subsidence and sedimentation rate (equation 9.17), and

the surface topography is irrelevant. On the other hand, as  $T \rightarrow 0$ , equation 9.12 behaves like the conventional diffusion equation involving only the surface elevation, and the subsidence becomes irrelevant. This can be summarized informally by saying that the slow changes are felt in the body of the basin, whereas rapid changes are felt in its skin. Thus, rapid changes in subsidence rate produce no effect because the term they control is not that important in the short-term balance. Another way of looking at it is that, for changes in the subsidence rate to affect sedimentation pattern, sediment must be redistributed across the whole basin, which cannot happen on time scales less than the equilibrium time.

On the other hand, slow changes in water supply (diffusivity) have no effect because they influence only the sediment surface, which is not an important element in the long-term balance equation 9.17. Changes in water supply cause the sediment surface to rearrange itself slightly but do not affect the basic mass balance in the basin. Nonetheless, at short time scales, surface effects predominate because changes in water supply have a strong effect on surface configuration, and they strongly influence the pattern of sedimentation.

Finally, changes in sediment flux are effective on both time scales because the sediment flux affects both the overall mass balance of the basin and the surface topography. The latter effect is through the boundary condition (equation 9.13a). The reversal in form of the effect of varying flux as the time scale changes results from competition between the effect of the flux on the mass balance and on the sediment surface. Over long time scales the mass-balance effect is more important, whereas on short time scales, the surface effect predominates. Note also that, because the effect of the flux on the sediment surface is produced at the edge of the basin and then propagates inward, the argument made above about reduced length scales comes into play. The length scale  $L'$  over which the variation in flux can be expected to propagate goes as  $R(T)$ , so variation on a time scale that is 1/10 of the equilibrium time should be concentrated in the upstream-most 30 percent or so of the basin. That this is indeed the case can be seen from inspection of Figure 9.10a. The gravel front propagates much farther into the interior than this; however, because of the dramatic increase in apparent gravel flux as the gravel-rich upstream deposits are eroded.

## G. COMPARISON WITH FIELD RESULTS

At this time, it is not possible to test the results of models such as ours directly against field data. To do this, we need to know the migration history of grain-size fronts through time as well as other independent variables of the system, and such data are not available at present. Nonetheless, we can compare the overall model results with existing data on grain-size changes in basins. In particular, we can test the predicted results for quasiequilibrium changes against field data, because age control need not have as high a resolution as that required for nonequilibrium conditions. Specifically, we can determine if gravel progradation is caused by an increase in sediment flux or a decrease in subsidence. This is an important distinction in interpreting the sedimentary record because the flux-driven case suggests that tectonic uplift of the source area was the major control on deposition (i.e., synorogenic conglomerate), whereas the subsidence-driven case corresponds to a time of a reduction in tectonic loading (i.e., nonorogenic conglomerate).

To test this model, we must focus on coarse progradational sequences that occurred over sufficiently long time periods to be in quasiequilibrium (of the order of  $10^6$ - $10^7$  yr). In addition, relatively high-resolution age control must be available from the same vertical sequences that the grain-size data come from. Fortunately, these data exist in published magnetostratigraphic studies of alluvial sequences in a few settings. Although these data sets are few, they unequivocally demonstrate the flux-driven and subsidence-driven models.

### 1. *Example of Flux-Driven Sedimentation*

Neogene deposits of the Bermejo foreland basin, in La Rioja province of northwest Argentina (Beer and Jordan, 1989), provide an example of flux-driven gravel progradation. At Las Juntas, a site within the Precordillera thrust belt, Reynolds et al. (1990) used a thick (4780 m) coarsening-upward sequence to determine tectonic timing in the adjacent thrust belt. The section was deposited between about 18 and 10 Ma and overall coarsens upward from siltstone and sandstone to conglomerate (Fig. 9.11). Vertical sediment accumulation rates calculated from the magnetostratigraphy (Reynolds et al., 1990) show a general increase

upsection as the section also becomes increasingly coarse-grained (Fig. 9.11). Although the increase in sedimentation rate is small (from about 0.3 to 1.3 mm/yr), this positive correlation indicates flux-driven gravel progradation, indicating that this gravel unit is tied to an increase in sediment being delivered to the basin. The authors' interpretation of tectonic uplift and erosion of the source area (Reynolds et al., 1990) is in agreement with the results of our model and suggests that this progradation does represent synorogenic deposition.

Although this is the only example of clearly flux-driven sedimentation known to us in the literature, note that the traditional interpretation of gravel progradation is that it is indicative of tectonic events resulting from an increase in sediment supply (e.g., (Rust and Koster, 1984; Steel et al., 1977; Van Houten, 1974). The flux-driven model represents the classical synorogenic interpretation of progradational sequences in alluvial basins.

## *2. Example of Subsidence-Driven Sedimentation*

An excellent example of subsidence-driven sedimentation is provided by the work of Burbank and his colleagues over the past few years from the Northwest Syntaxis of the Himalayan foreland basin (Burbank et al., 1988; Burbank et al., 1986). A series of magnetostratigraphic sections from the Siwalik Group, measured more than 80 km basinward of the source area in the Pir Panjal Range and Kashmir Basin sector of the Himalayas, shows a sequence that coarsens upward from fluvial molasse sandstones to conglomerates between 4 and 1 Ma (Fig. 9.12). For this sector of the Himalayan foreland basin, a reasonable response time is on the order of 1 My. Vertical sediment accumulation rates, calculated from the magnetostratigraphic data, show that a general decrease takes place prior to or as the overall grain size increases into gravels (Fig. 9.12). Burbank et al. (1988) note this relationship and attribute the progradation in this sector to a decrease in subsidence, in agreement with our model results. Also, Burbank et al. (1988) suggest that in the more proximal part of the basin progradation was apparently coupled to an increase in sediment flux and not to reduced subsidence rates. If correct, then the main mechanism that causes gravel to prograde across the basin should shift over time from increasing sediment flux to diminishing subsidence.

However, data from the more proximal part of the basin are lacking and several other explanations may also account for this observation. Regardless, it is important to note that although the Himalayas discharge large volumes of sediment into the basin, which is augmented by longitudinal sediment transport systems (Burbank et al., 1988), it is still subsidence that drives the conglomeratic progradation in, at least, the part of the basin where data are available. Therefore, the presence of gravels in these sections (Fig. 9.12) correspond to a time of diminished subsidence, and so, assuming that subsidence is directly a product of thrusting in along the Main Boundary Thrust, they represent times of relative tectonic quiescence and are not synorogenic.

#### H. FUTURE DIRECTIONS IN STRATIGRAPHIC MODELING

Our basic aims in this chapter have been to show you how a basic model of fluvial basin filling is constructed and to examine some of the results produced by the model. Even if you do not pursue this type of modeling yourself, we hope that you will find the various response patterns shown in Figures 9.8 through 9.10 stimulating to think about.

What are likely future directions for basin modeling? We see two major directions of research developing over the next few years: (1) development of new methods of independently estimating the parameters in quantitative models, and (2) elaboration of existing models to make them more realistic (and more complicated). Both of these efforts will involve close collaboration between field workers and modelers.

We consider as an example of the problems of estimating the independent variables the estimation of water discharge. The modeling makes clear the basic role played by the long-term average water discharge in governing basin behavior, via the diffusivity. The diffusivity, in turn, is not only an important variable in its own right, but its mean value helps determine the response time, which is critical in determining how variation of any parameter will affect basin sedimentation. One of the great challenges of applying quantitative models to the interpretation of ancient sediments is to find ways of estimating the diffusivity. Two possible lines of approach come to mind: (1) paleoclimatic estimation of rainfall rates (from paleosol studies) coupled with tectonic constraints

on the size of the ancient drainage area, and (2) paleohydraulic reconstruction of flow rates in ancient river systems. The first method gets directly at the critical parameter (the long-term average water supply rate), but is apt to be imprecise. As for method 2, although fairly precise paleohydraulic reconstructions of specific paleoflow events are possible, it is not clear how these can be suitably integrated to give an estimate of long-term water supply. Although neither approach seems workable at present, we think that the pursuit of either offers an appealing way of quantitatively integrating small-scale sedimentological studies with regional basin analysis.

What kind of improvements can we expect to existing models? Some of the lines along which efforts are being made now include development of three-dimensional models, incorporation of more detailed models of sediment transport and fluid dynamics, and incorporation of stochastic effects in the models. All of these refinements can be made within the framework of models such as the one described here, but other approaches are also possible. One of particular interest is that taken by Tetzlaff and Harbaugh (1989). They have developed a set of elaborate computer codes that simulate sedimentation in basins by following the movements of individual fluid elements, using a computational technique called the marker-in-cell method. The fluid elements are launched at a fixed rate from a source; after that, their behavior is determined by approximations to the governing equations. This method is appealing for several reasons. Probably the strongest reason is that it can produce river, delta, and turbidite systems, and associated deposits that are both three-dimensional and strikingly realistic-looking, with minimal user input. The flows migrate and avulse in an apparently random way, and the simulated deposits strike the eye as capturing at least some of the complexity of real deposits. At the moment, one main drawback of this method is that it is almost entirely untested. It has not yet been applied to modeling the behavior of any active modern systems, where its predictions can be compared with measurements. Another drawback is that it is very complex computationally, which means among other things that it may be difficult to understand the basic physical meaning of the model results. Nonetheless, it is a promising technique that bears watching.

It is worth keeping in mind that the quantitative modeling of sedimentary basin filling began in earnest only in the last few years. It is difficult to predict what basin-filling models will look like ten years from now. Regardless of which modeling strategy ultimately turns out to be best, the complexity of the calculations involved means that the evolution of basin-filling models is apt to be strongly influenced by the evolution of computer hardware. However, the availability of field data, especially high-resolution chronostratigraphy, will be a more significant limiting factor in model development than the availability of computational power.

## 10. SUMMARY

In this course we have summarized the techniques of quantitative basin analysis from the standpoint of modeling subsidence histories and mechanisms. We recommend becoming familiar with successful basin studies that have used these techniques to more fully understand the concepts that are only briefly covered here. The reference list accompanying these short course notes provides many, but by no means all, examples of subsidence analyses and will serve as a good starting point for more intense study. We also recommend attempting a subsidence analysis of your own on any basin of interest. The application of these techniques to basin analysis studies provides a relatively new, but very powerful, tool to understanding the role of tectonics and sea level in the formation of a sedimentary basin.

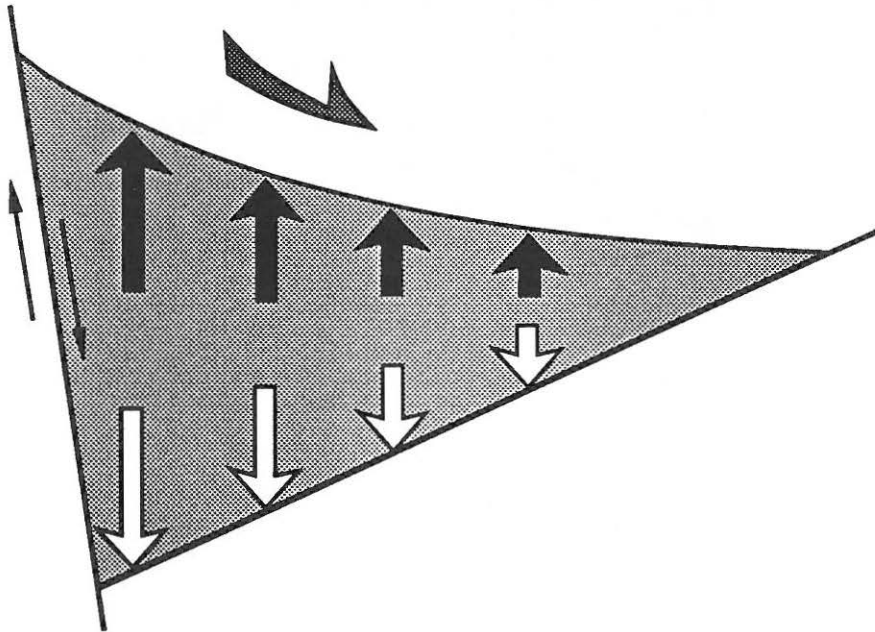


Figure 9.1 Cross section of a basin at equilibrium: subsidence (open arrows) and sedimentation (filled arrows) are in balance. Transport direction shown by curved arrow. Fault offset is shown with small arrows.

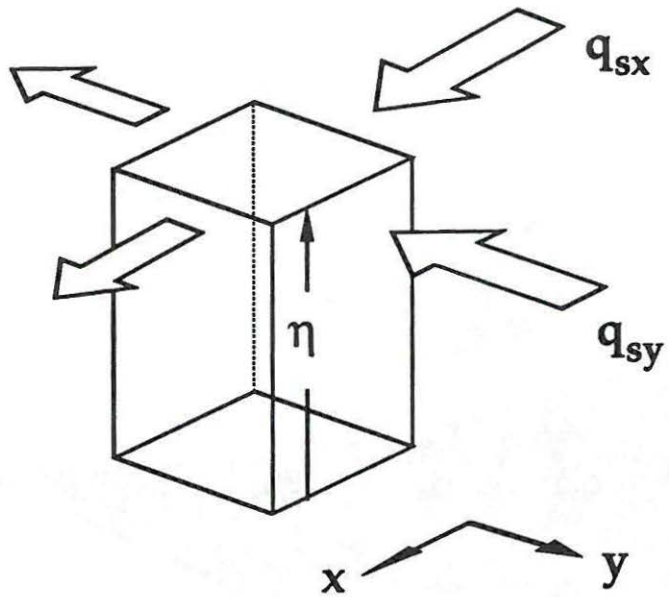


Figure 9.2: Definition sketch for conservation of sediment mass in two dimensions. Symbols are defined in the text.

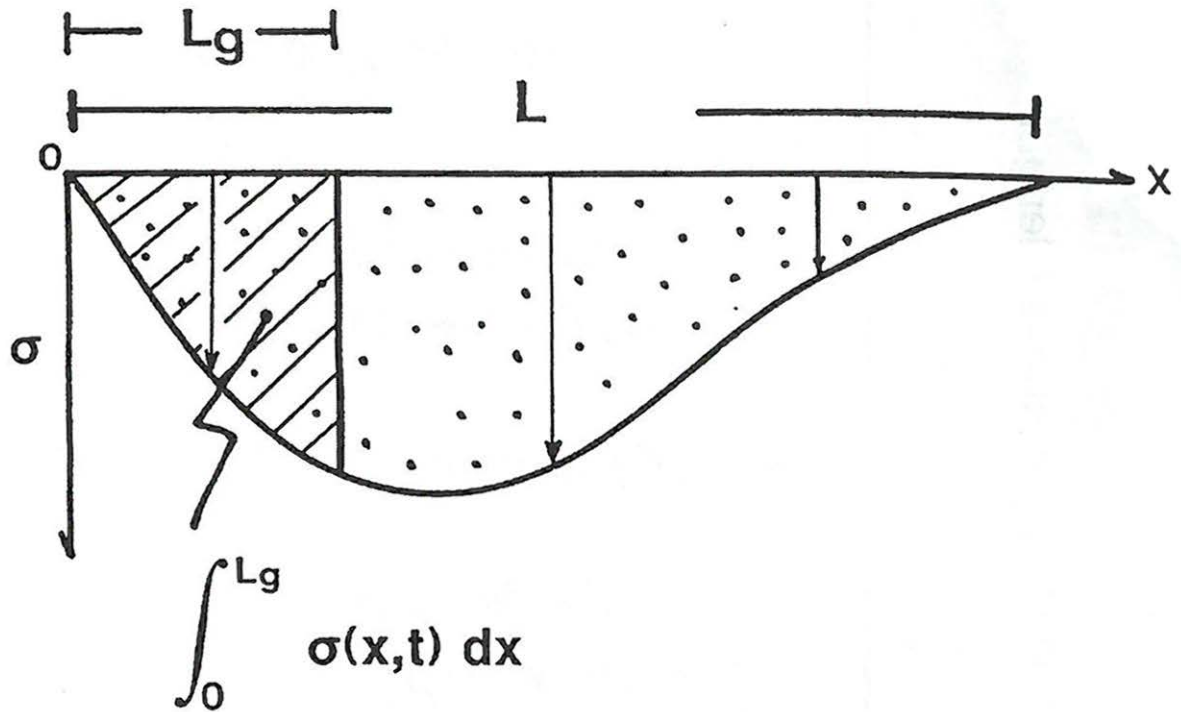


Figure 9.3 Factors determining the gravel transport distance  $L_g$  for the case  $R = 1$  (sediment supply equals subsidence). The vertical axis  $\sigma$  is the subsidence rate. The dotted area is the total area created per unit time. The diagonally ruled area is the area filled with gravel per unit time, equal to the volume rate of gravel supply per unit width and time. The length of the gravel-filled area is  $L_g$ . After Paola (1988).

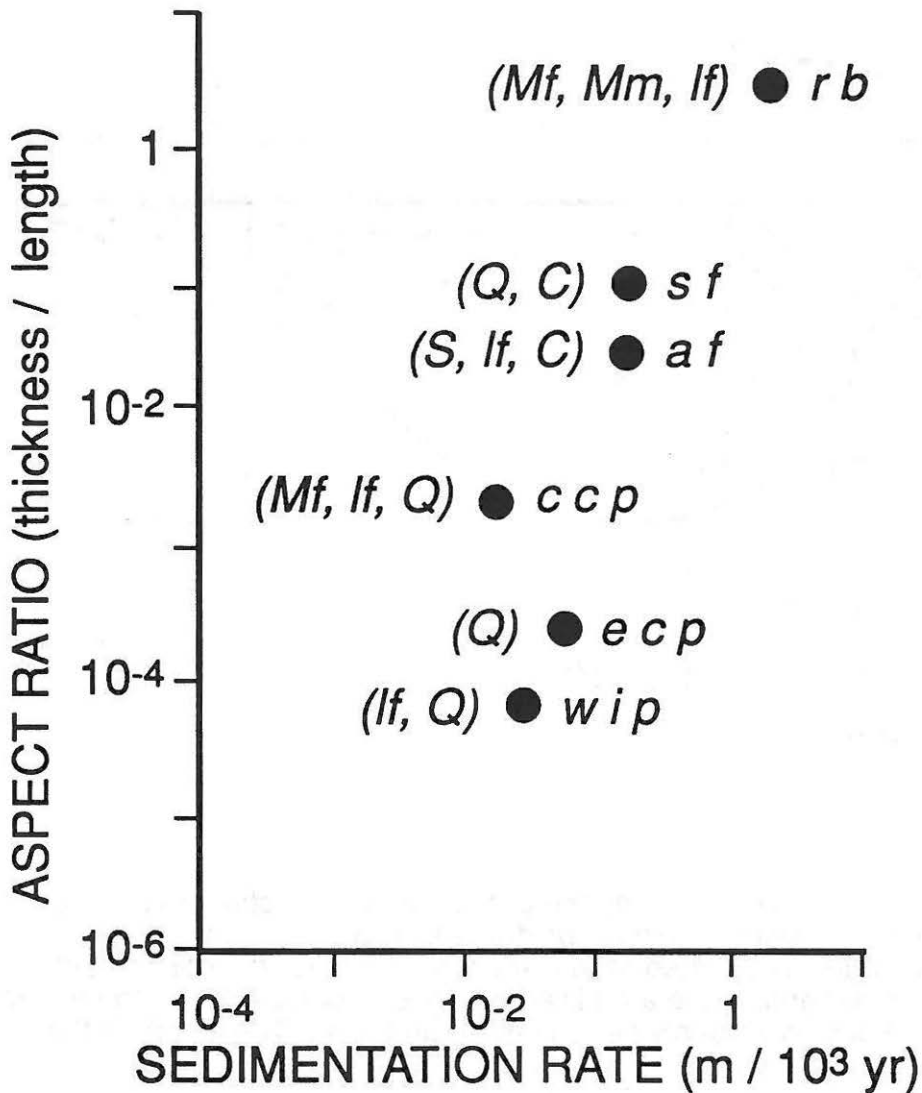


Figure 9.4 Variation of cross-sectional shape of gravel bodies with sedimentation rate. Dominant clast types are given in parentheses: Mf = felsic metamorphic, Mm = mafic metamorphic, lf = felsic igneous, C = carbonate, Q = quartzite and chert, S = other sedimentary rocks. Basins: rb = Ridge Basin, California, Upper Miocene (Crowell, 1982; Ensley and Verosub, 1982); sf = Sevier foreland, western interior, U.S.A., Albian-Santonian (Lawton, 1986); af = Alpine foreland, Switzerland, Chattian - Aquitanian (Trümpy, 1980); ccp = southern California coastal plain, Upper Eocene (Minch, 1979; Steer and Abbott, 1984); ecp - central Atlantic coastal plain, U.S.A., Pliocene (Schlee, 1957); wip = western interior alluvial plain, U.S.A., Pleistocene (Stanley and Wayne, 1972). After Paola (1988).

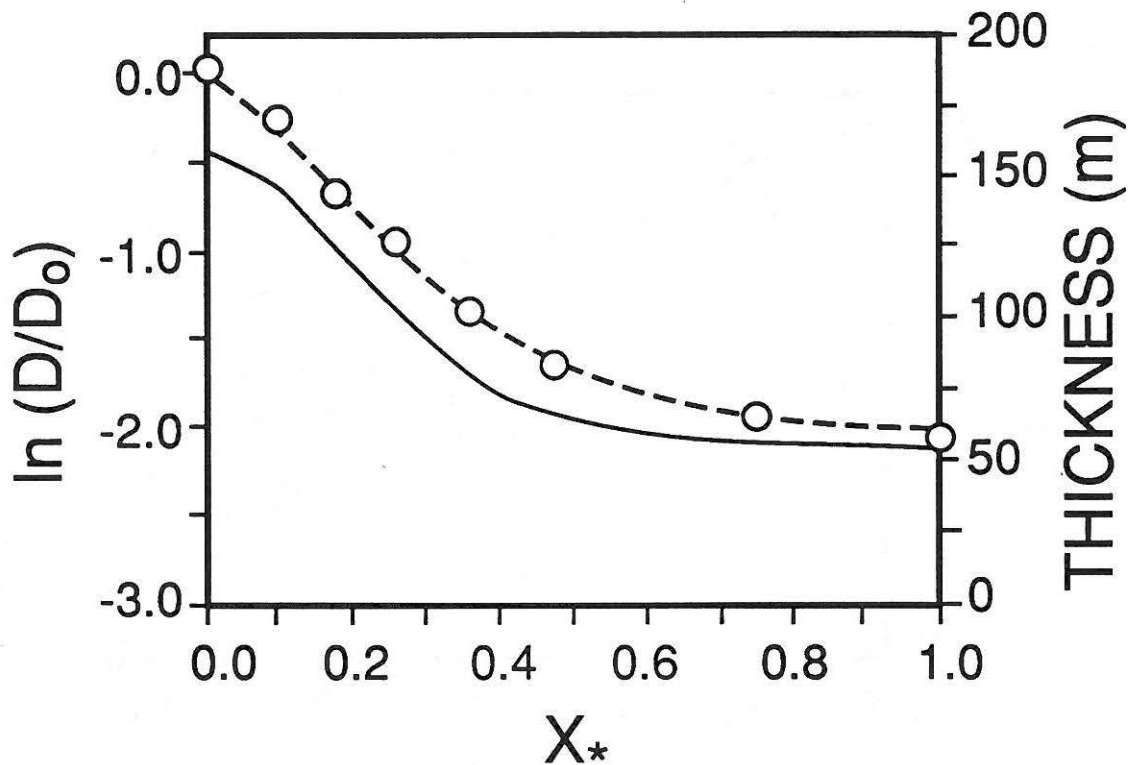


Figure 9.5 Grain size and sediment thickness as functions of downstream distance for Silurian rocks of eastern Pennsylvania.  $D$  is grain size relative to its value  $D_0$  at the upstream end of the basin;  $X_*$  is downstream distance relative to total basin length. Open circles show grain-size data, the dashed line shows the data trend, and the solid line is sediment thickness. Data of Yeakel (1962); figure after Paola (1988).

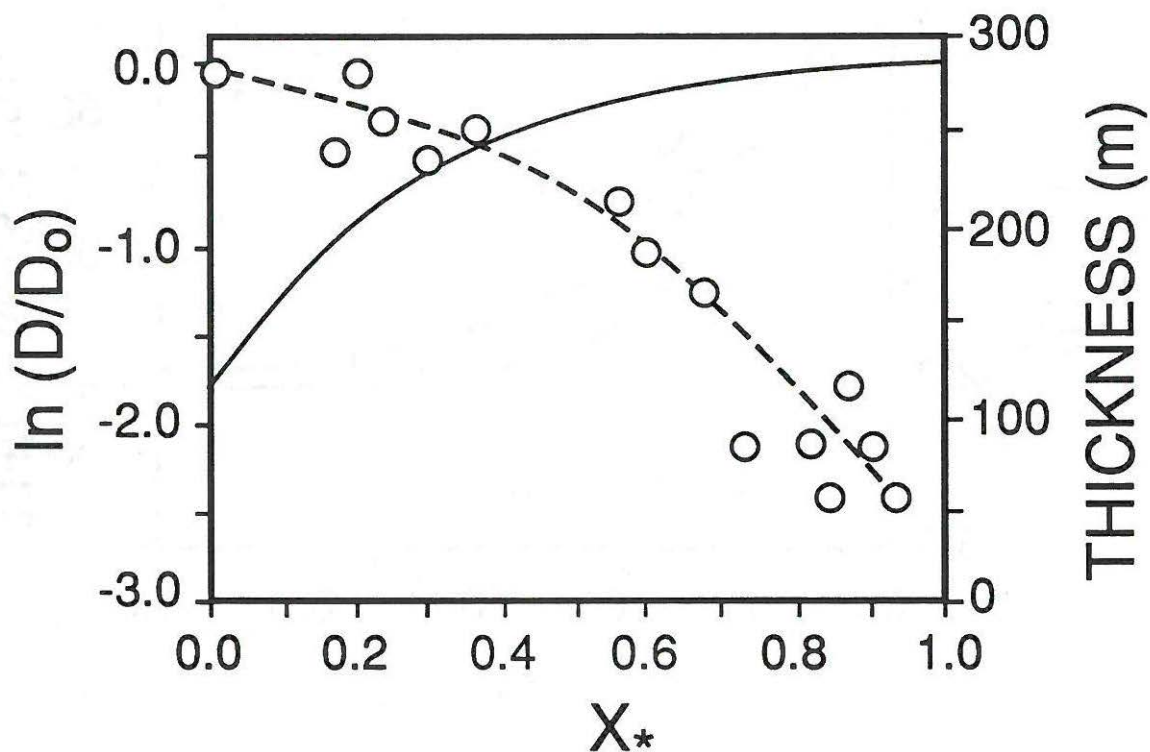


Figure 9.6 Grain size and sediment thickness as functions of downstream distance for Triassic rocks of southern Germany.  $D$  is grain size relative to its value  $D_0$  at the upstream end of the basin;  $X_*$  is downstream distance relative to total basin length. Open circles show grain-size data, the dashed line shows the data trend, and the solid line is sediment thickness. Data of Forche (1935); figure after Paola (1988).

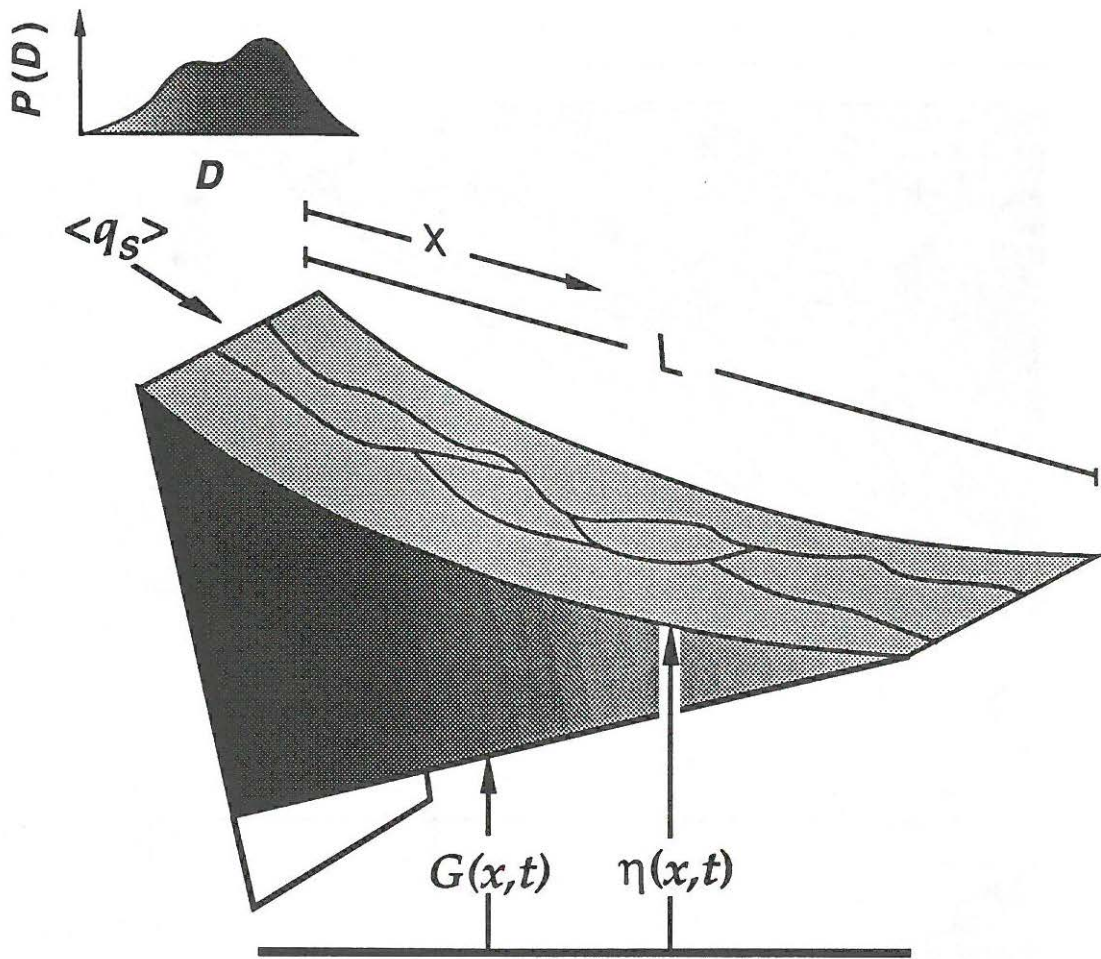
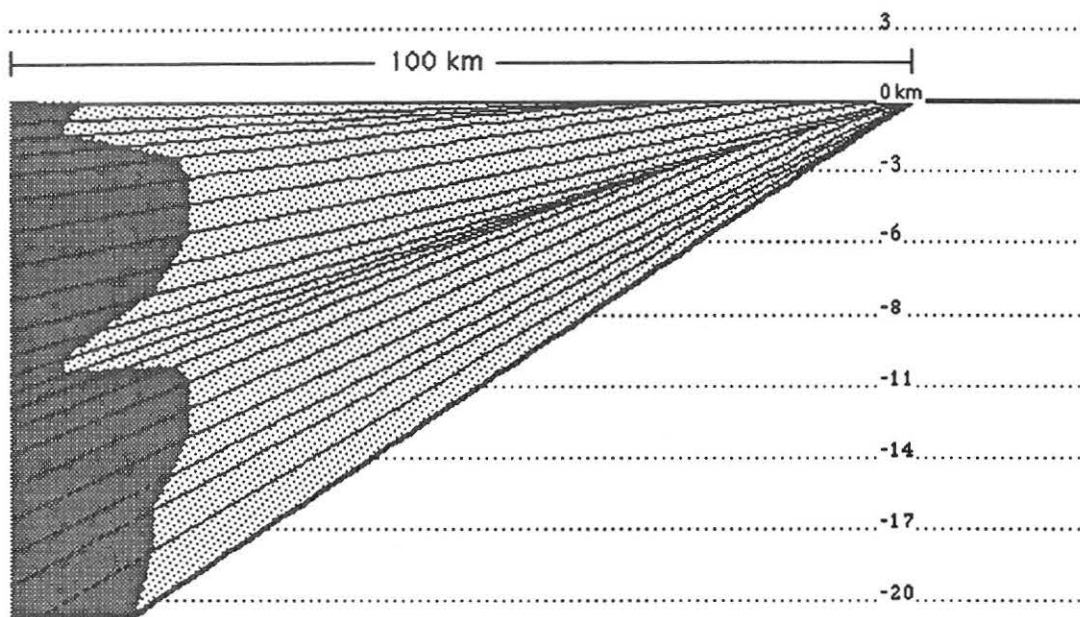


Figure 9.7 Definition sketch of a two-dimensional slice of a sedimentary basin. See text for explanation.

Please insert this page for figure 9.8

A.

E R R A T U M



B.

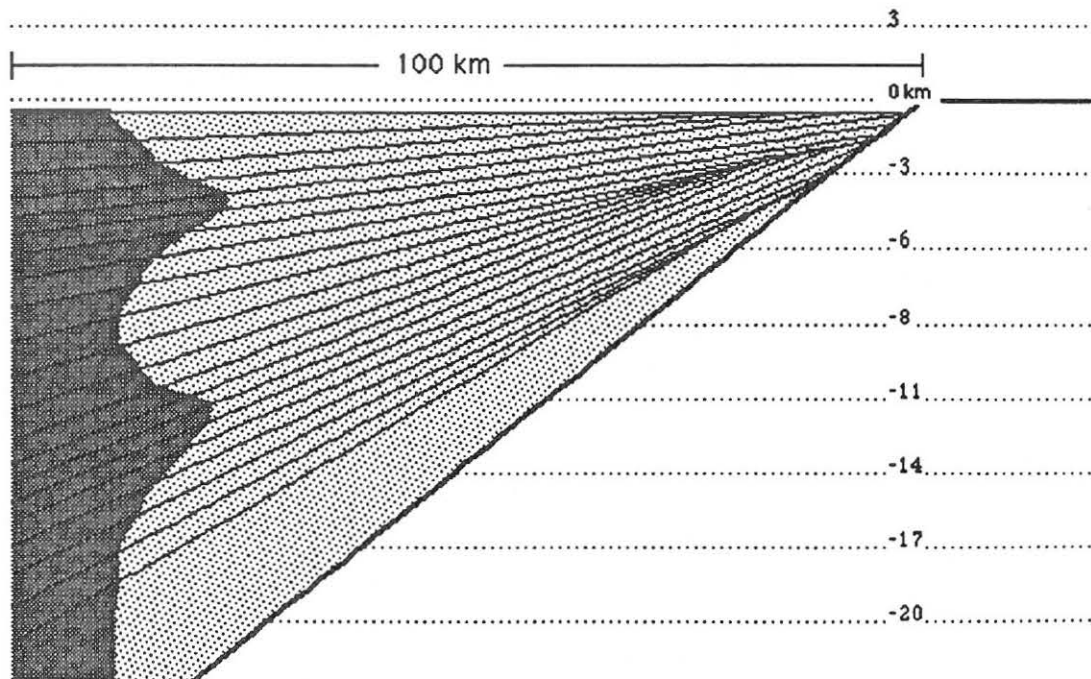
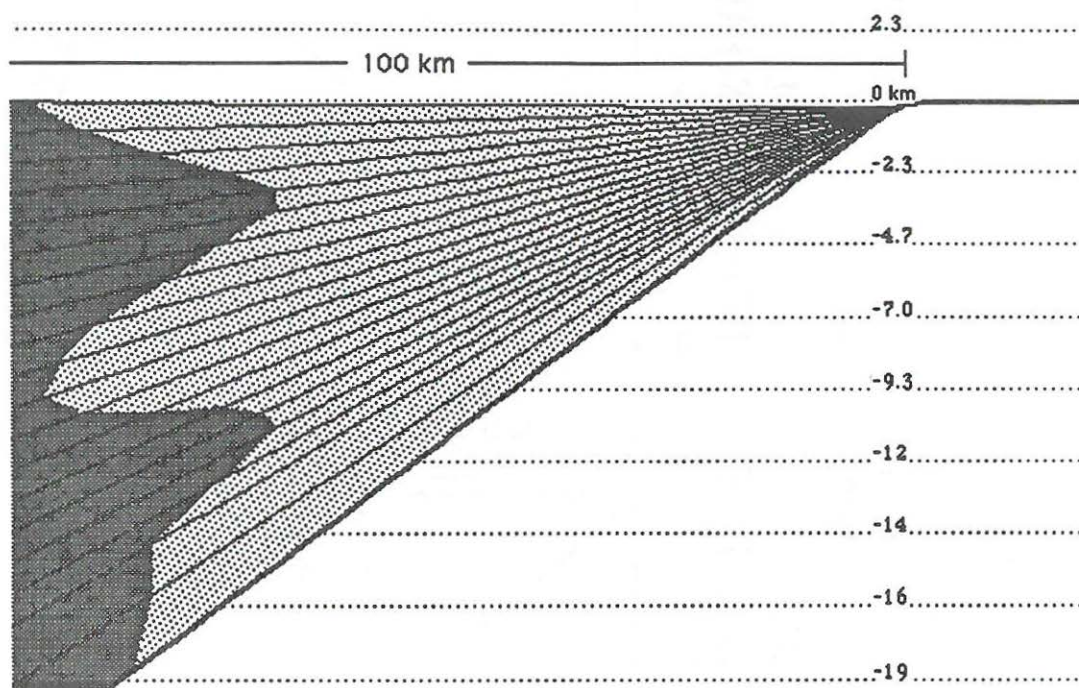


Fig. 9.8 Cross-sections of a hypothetical basin showing the results of slow variation in (A) sediment flux, (B) subsidence, (C) gravel fraction, and (D) diffusivity. Gravel is shown in dark gray, sand in light stipple. Direction of transport is from left to right. The light lines are isochrons drawn every  $10^6$  yr; the heavy lines show the basement surface. See text for the conditions of the run. All dimensions are in kilometers.

# C.



# D.

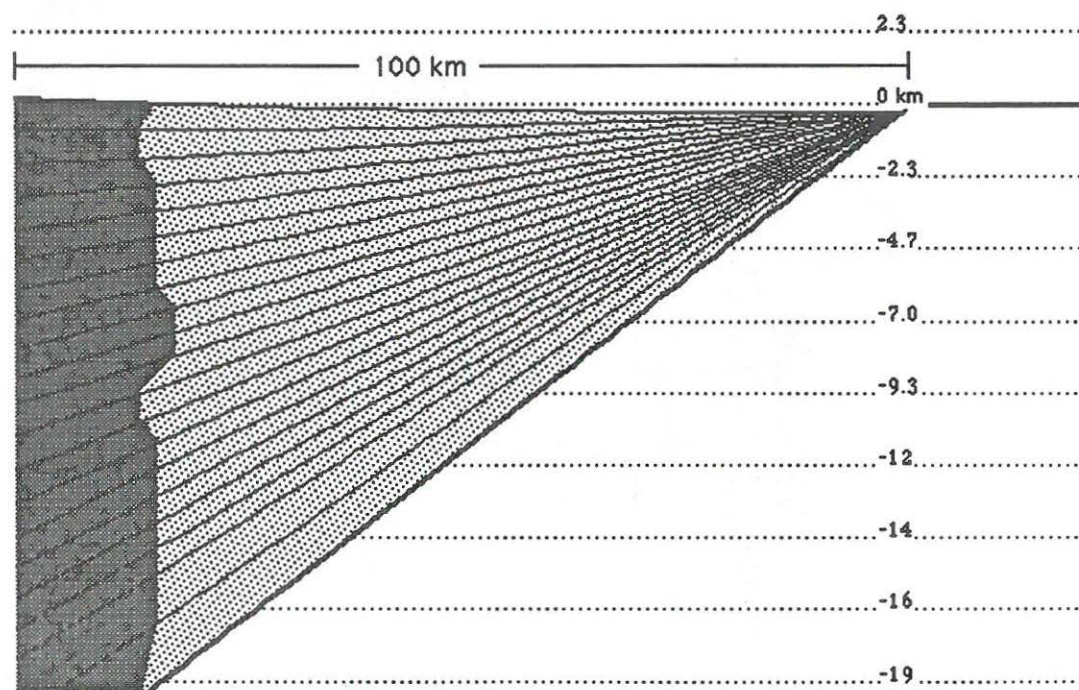


Fig. 9.8 (continued)

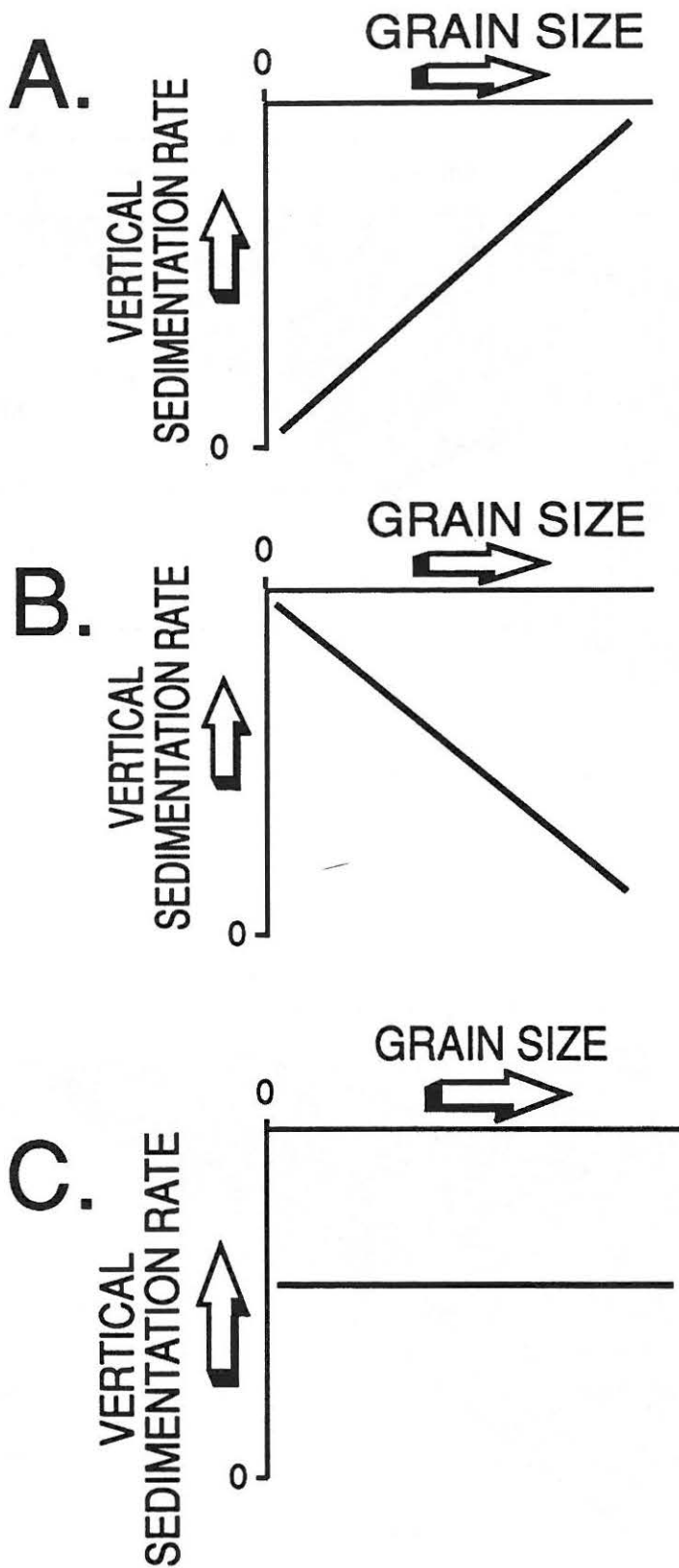


Figure 9.9 Idealized graphs showing the relation between grain size and local vertical sedimentation rate for (A) flux-driven , (B) subsidence-driven,) and (C) distribution-driven coarsening.

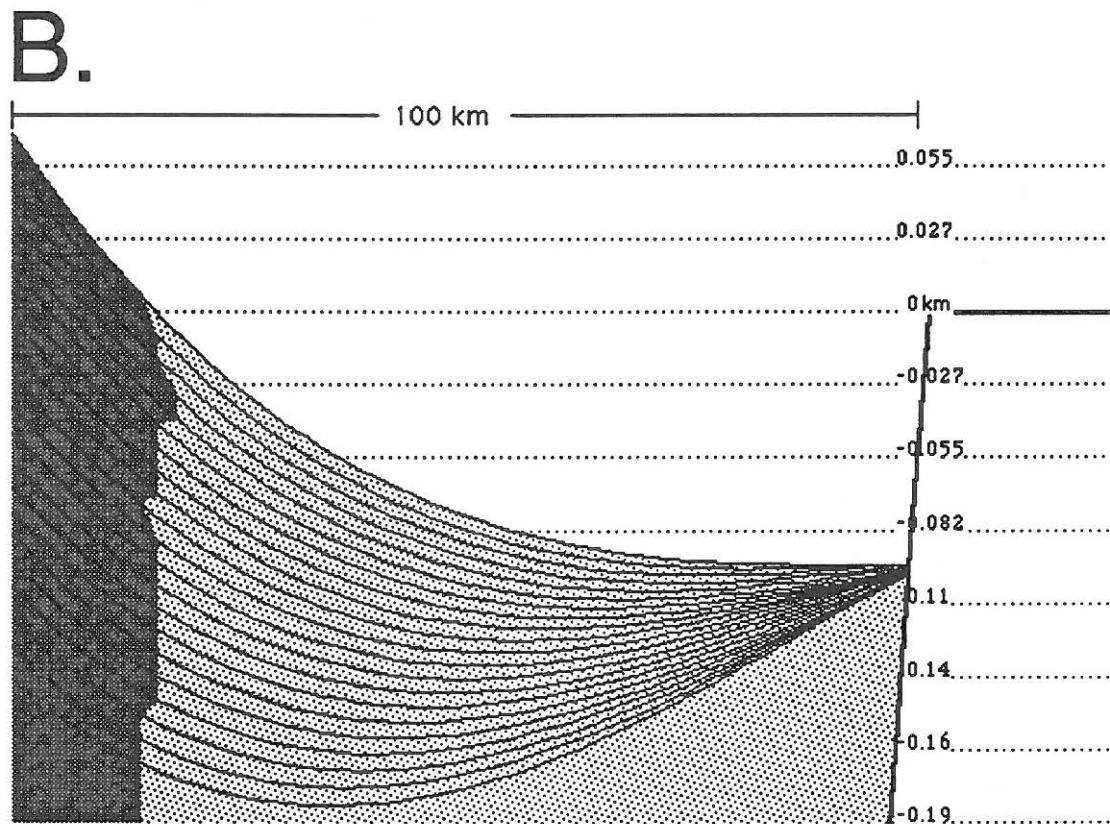
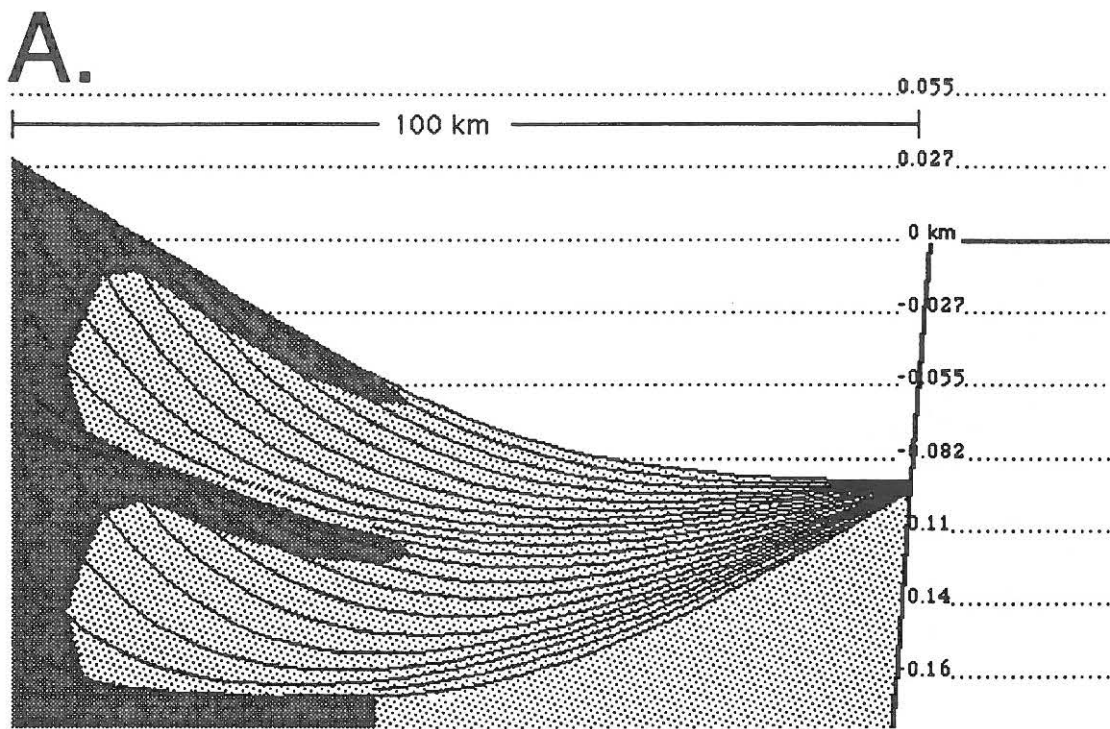
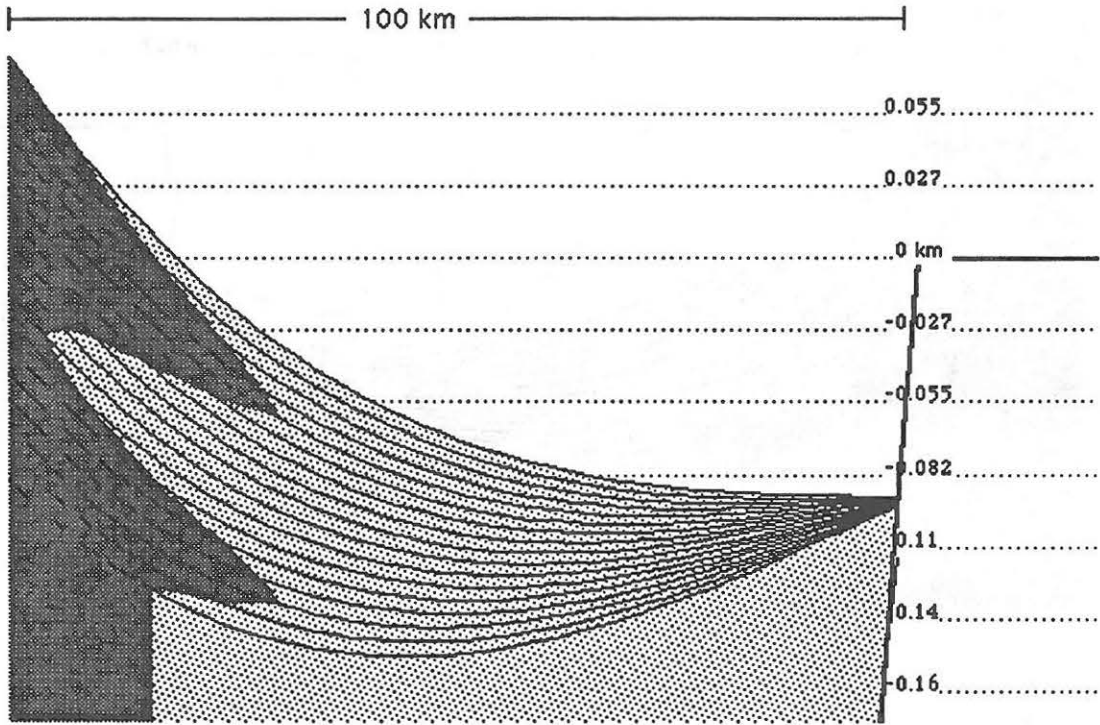


Fig. 9.10 Cross-section of a hypothetical basin showing the results of rapid variation in (A) sediment flux, (B) subsidence, (C) gravel fraction, and (D) diffusivity. Gravel is shown in dark gray, sand in light stipple. Direction of transport is from left to right. The light lines are isochrons drawn every  $10^4$  yr; the heavy lines show the basement. See text for conditions of the run. All dimensions are in kilometers.

C.



D.

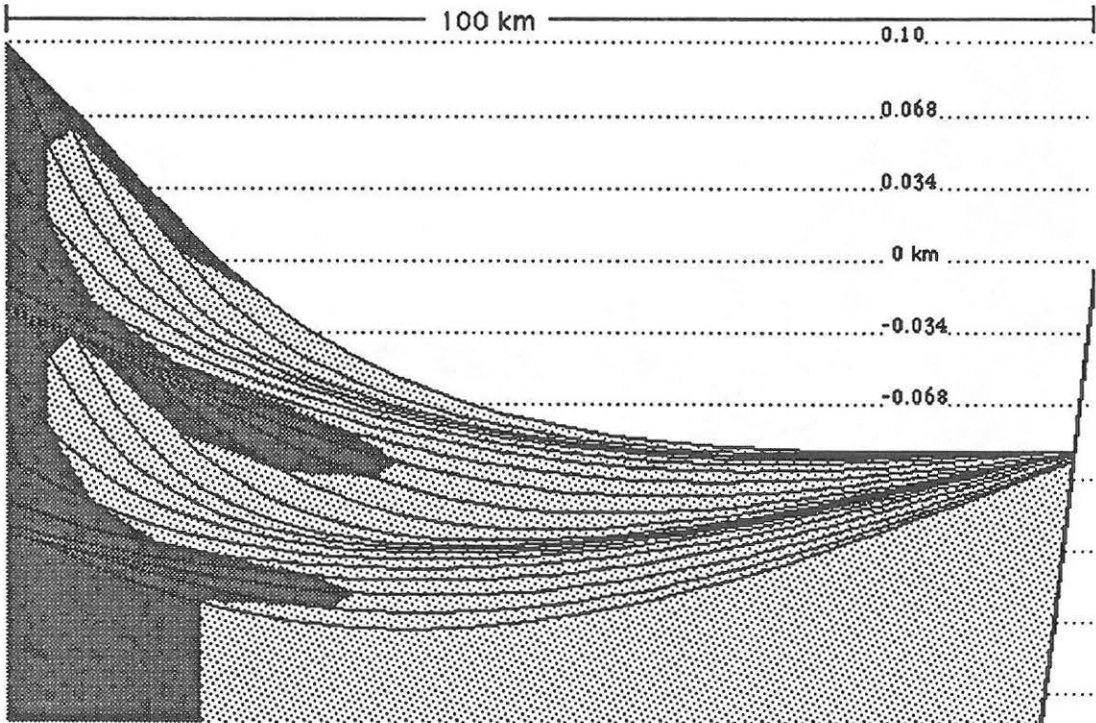


Fig. 9.10 (continued).

## *Las Juntas, Argentina*

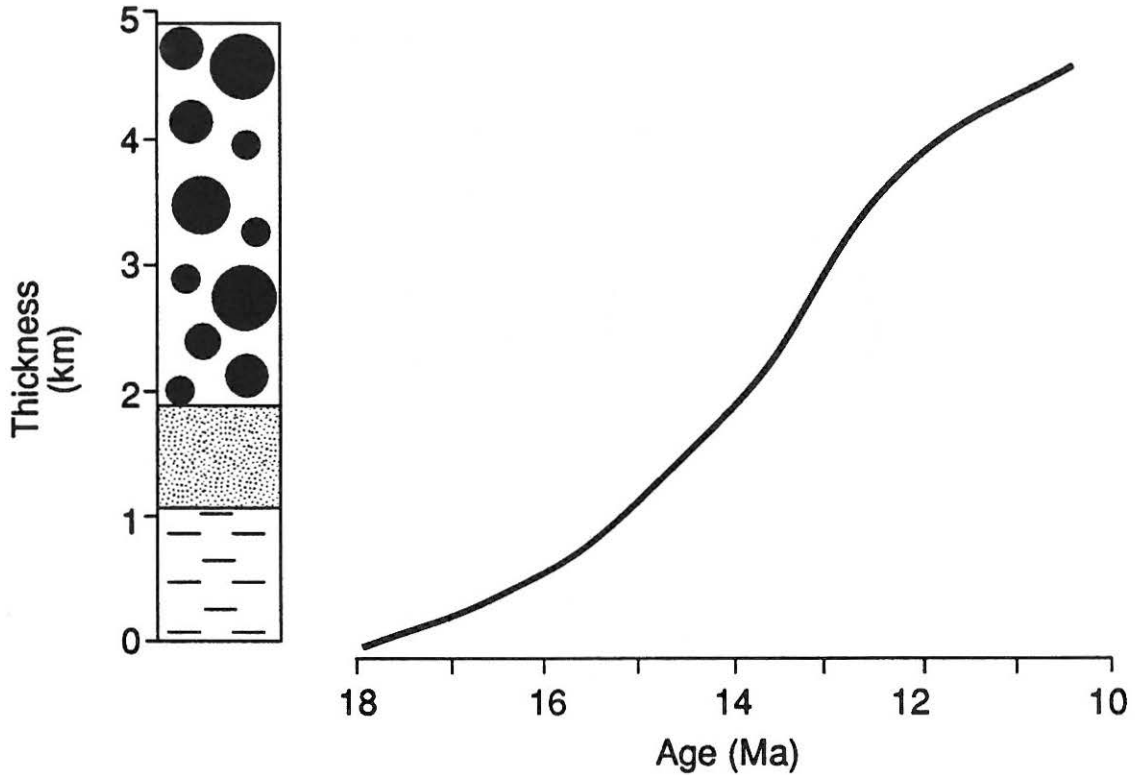


Figure 9.11 Decompacked sediment accumulation and lithofacies from Las Juntas, Argentina. Sediment accumulation and lithofacies data from Reynolds et al. (1990). Note that lithologies coarsen upsection from siltstone and sandstone (dashed and stippled patterns, respectively) to conglomerate and sandstone (solid dots) as sedimentation rates increase.

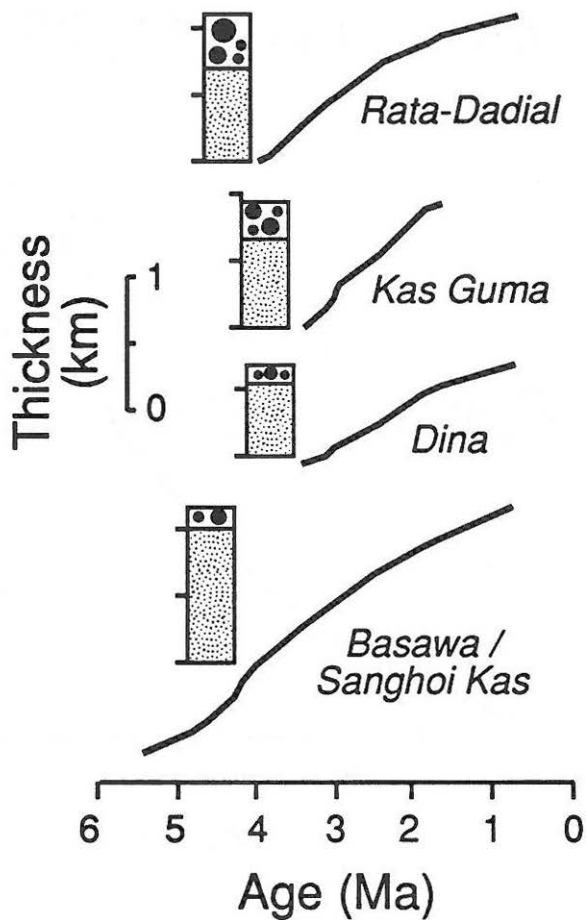


Figure 9.12 Decompressed sediment accumulation and lithofacies from four localities in the Himalayan foreland. Sediment accumulation and lithofacies data from Burbank et al. (1988). Note that lithofacies coarsen upsection from fluvial molasse facies (stippled) to gravelly facies (solid dots) after sediment accumulation rates decrease circa 3 Ma.